2019 IEEE/RSJ International Conference on Intelligent Robots and Systems (IROS)
Macau, China, November 4-8, 2019

Reconstructing Endovascular Catheter Interaction Forces in 3D using Multicore Optical Shape Sensors

Christoff M. Heunis, Vincenza Belfiore, Marilena Vendittelli and Sarthak Misra

***Abstract*— Catheterization instruments are increasingly being improved to accurately diagnose and treat cardiovascular conditions. However, current catheter systems provide limited information about the shape of the catheter and tissue-instrument interaction forces during an intervention. Furthermore, relying on inconsistent feedback of such interaction forces during an intervention may result in tissue injury. This paper presents the first steps to estimate the interaction forces between a catheter and a mock-up arterial environment. We base the proposed method on a Pseudo-Rigid Body approximation of the catheter and integrate three-dimensional shape information provided by Fiber Bragg Grating sensors inside the catheter. The reconstructed forces along the catheter body can be fed back to the surgeon in visual and/or haptic form. In this work, the estimated forces are displayed in real-time in a graphical user interface with the reconstructed catheter shape. Experimental validation demonstrates a root mean square error of 0.03 N and a mean reconstruction error of 0.02 N.**

***Index Terms*— Force and Tactile Sensing, Simulation and Animation, Surgical Robotics: Steerable Catheters/Needles,**

I. INTRODUCTION

ENDOVASCULAR interventions are increasingly being used to treat heart conditions and problems affecting blood vessels, such as aneurysms, coronary artery diseases, and arteriosclerosis. The need to aid with the treatment of these conditions has fostered the development of a wide variety of flexible instruments driven by robotic manipulators [1]. The integration of robotic systems with surgery is becoming increasingly popular, as it allows clinicians to complete complex surgical techniques with more precision, flexibility, and control concerning conventional manual techniques. Recently, steerable catheters have been developed to aid in endovascular procedures. However, interaction forces between the blood vessel and the catheter sometimes hamper vascular catheterization procedures (Fig. 1).

Such forces can induce tissue damage, vasoconstriction and result in reactive intimal proliferation or distal embolization [2]. Another complication is the loss of force information which the catheter exerts unto blood vessel walls through its tip and along the catheter body [3]. Having accurate knowledge of these interaction forces between the catheter and tissue is important to provide force feedback and, given the appropriate actuation techniques, to reduce tissue damage [4].

Christoff M. Heunis and Sarthak Misra are affiliated with the Surgical Robotics Laboratory, Department of Biomechanical Engineering, University of Twente, The Netherlands. Sarthak Misra is also affiliated with the Department of Biomedical Engineering, University of Groningen and University Medical Centre Groningen, The Netherlands.

Vincenza Belfiore and Marilena Vendittelli are affiliated with the Department of Information Engineering, Electronics and Telecommunications and with the Robotics Laboratory at the Department of Computer, Control and Management Engineering, Sapienza University of Rome, Italy.

This work is supported by funds from the Netherlands Organization for Scientific Research (Innovational Research Incentives Scheme - VIDI: *SAMURAI* project # 14855).

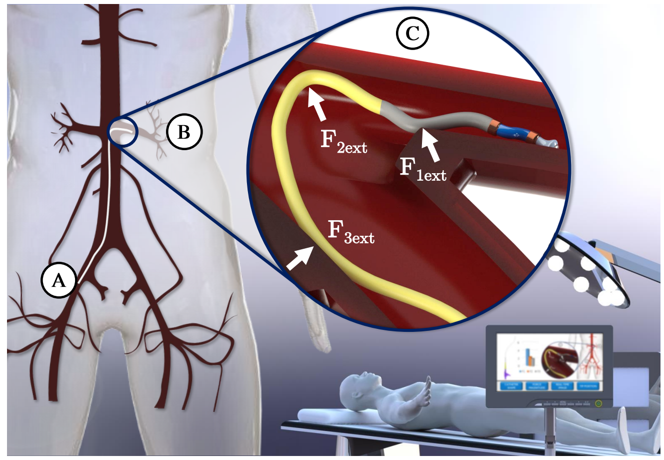

Fig. 1: A representative illustration of an endovascular catheter being guided from an insertion point, A, to a target location, B. The inset, C, shows the catheter inside the main arterial branch, being steered into the renal artery. Unpredictable forces acting along the catheter body, and at its tip ($F*_{ext}$, with $*$ denoting the number of contact points) may cause unnecessary damage to the blood vessel wall.

Various studies have proposed algorithms to estimate the interaction forces on the manipulator without measuring them directly [5]–[8]. For instance, Khosnam *et al.* utilized the curvature of a catheter, determined from camera images, in combination with a kinematic model in order to estimate the tip contact forces [9]. Back *et al.* identified catheter tip forces using the Cosserat rod model and the catheter shape [10]. Shi *et al.* designed a functional miniaturized end-effector that integrates a piezoelectric actuator and a fiber optic sensor, to be used in minimally invasive procedures [11]. King *et al.* designed a piezoresistive tactile sensor integrated with a surgical instrument tip [12], which sparked the development of additional force-sensing functionalities in instrument tips, such as the grasping, pulling and cutting of tissue [13], [14].

However, current methods in the state-of-the-art are not clinically applicable, either due to sensor integration problems, or imaging modalities that are incompatible with clinical use. Furthermore, sensing forces accurately at the catheter tip is challenging, as the space inside the catheter does not allow for the integration of force sensors and, moreover, contact points along the manipulator body distort the information

978-1-7281-4003-2/19/$31.00 ©2019 IEEE

of interaction forces [5], [6], [15]. An alternative method to estimate such interaction forces is by utilizing shape sensors that are fitted directly on the manipulator body. Fiber Bragg Grating (FBG) sensors have shown great potential in shape and force sensing of continuum manipulators and biopsy needles [16]. These sensors are sensitive to changes in mechanical strains or ambient temperature, and these changes cause a shift in the reflected wavelength through an optical fiber. Previously, Yokoyama *et al.* presented a new sensor that detects and measures contact forces during cardiac ablation [17]. The force sensor (Touch+, Endosense) is integrated with a 7 Fr ablation cardiac catheter. Recently, Khan *et al.* estimated the external force at the tip of a tendon-driven continuum manipulator using the FBG sensor measurements in conjunction with a model of the manipulator, and a known contact point of the applied force [18]. Despite the significant progress made on shape sensing, it remains challenging to use these methods in order to provide an accurate estimation of unpredictable forces acting on the entire catheter body in an unknown environment.

This paper proposes the first of a two-phases approach toward the estimation of contact forces along the whole body of a 6 Fr (2 mm diameter) catheter. Specifically, an appropriate model of the catheter and the algorithm to estimate the considered interaction forces is provided. In this first phase, we assume to know these contact points. It is worth noticing, however, that in this framework, this assumption is not limiting since the information provided by the proposed algorithm can be exploited to identify the points of contact, in the line of [19] and [20] and it is the subject of ongoing research. In other words, the proposed method has the interesting property of being structurally susceptible to be extended to include the identification contact points.

Using multicore FBG sensors, we reconstruct the shape of the catheter that allows the estimation of environmental loads. This eliminates the need for dependent force sensors, which can be integrated with the catheter base, thereby reducing its size significantly. The catheter is approximated by a Pseudo-Rigid-Body (PRB) manipulator with passive elastic joints. To validate the method, the estimated forces are compared to the measurements of a 3D force sensor set at the catheter base. For the sake of illustration and further developments involving simulation studies, the experimental setup is reconstructed and displayed in a virtual robot experimentation platform (V-REP) environment [21].

The paper is organized as follows. After a preliminary description of the catheter modeling, Section II provides the method for the reconstruction of the contact forces along the entire shaft of the catheter. The experimental setup and catheter insertion experiments are presented in Section III. This is followed by the illustration of the data processing and of the obtained results in Section IV. Finally, Section V concludes the paper and provides directions for future work.

II. CONTACT FORCE ESTIMATION

A critical factor in reconstructing the forces on the catheter tip and along its shaft (hereinafter referred to as its body),

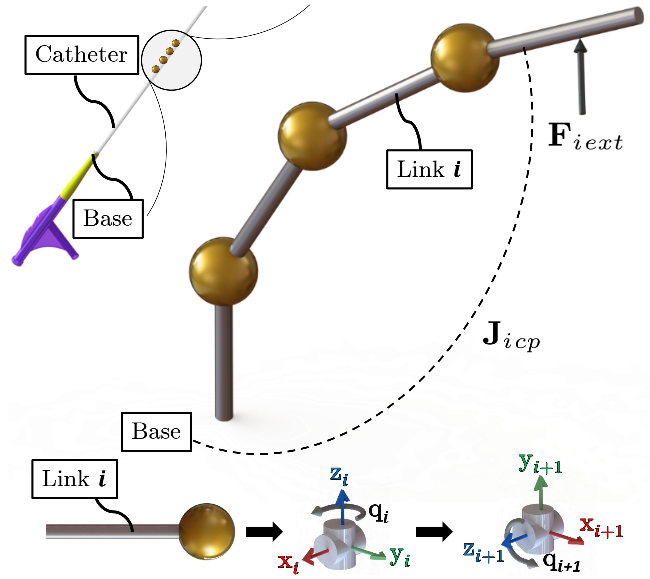

Fig. 2: The Pseudo-Rigid Body (PRB) model: Using the PRB modeling approach, the manipulator shaft can be approximated by a series of rigid links. The figure shows the approximation of a segment of the manipulator comprising four rigid links connected by three joints, with each joint having two degrees of freedom represented by the joint angles (q_i) and (q_{i+1}). $\mathbf{J}_{icp}$ is the contact point Jacobian relative to an unknown external force ($\mathbf{F}_{iext}$), acting on link (i). Multiple contacts are possible, although not illustrated in the figure, for the sake of legibility.

is to geometrically determine the tip position and joint coordinates. In this section, we describe the adopted Rigid Link Model of the catheter, and then how shape reconstruction and force sensing are integrated with our approach.

A. Pseudo-Rigid Body model

Endovascular manipulators have a mechanical structure analogous to that of continuum manipulators. Continuum manipulators can be modeled as a series of rigid links connected by passive elastic joints [22]–[26]. We consider a manipulator fixed at the base, experiencing forces along its body and tip in three-dimensional space. We propose to approximate the manipulator mechanics with a computationally fast PRB Model in order to estimate and render these contact forces. The interaction forces along the manipulator are determined based on the joint torque in static equilibrium. These joint torques are calculated from strain measurements provided by an FBG fiber inside the manipulator body. The manipulator id assumed to be torsionally rigid.

B. Kinematics

The kinematic chain used to describe the manipulator deformation (or shape) under the action of interaction forces or loads is illustrated by Fig. 2. In our case, the manipulator is approximated by a serial chain of *n*+1 rigid links connected by *2n* revolute joints. We consider a manipulator of length (l) equal to 340 mm. To avoid damage to the fiber, we limit our maximum link deflection to an arc radius of 10 mm. In the central lumen of our manipulator, we have a fiber consisting of 31 FBG sensors. The model comprises two joints for each sensor, hence 62 revolute joints. Link 0

TABLE I: Denavit-Hartenberg parameters of the manipulator used to approximate the catherer.

i	α_i	a_i	d_i	q_i
1	$\pi/2$	0	0	q_1
2	$-\pi/2$	0.101	0	q_2
3	$\pi/2$	0	0	q_3
4	$-\pi/2$	0.101	0	q_4
$\vdots$	$\vdots$	$\vdots$	$\vdots$	$\vdots$
61	$\pi/2$	0	0	q_{61}
62	$-\pi/2$	0.0183	0	q_{62}

is the base of the manipulator, fixed to the ground frame, and Link (n) represents the manipulator tip. We describe the geometry of our manipulator with the relative Denavit Hartenberg parameters in Table I. The joint angles (q_i) and (q_{i+1}) represent the degrees of freedom (DOF) of each joint. In the next sub-section, we relate the manipulator shape to external forces applied along the manipulator body and at its tip.

C. Statics and manipulator load analysis

In order to reconstruct the external forces, they need to be related to the shape of the manipulator. This shape is provided by processing data obtained from the FBG sensors. In static equilibrium, the loads that act on the manipulator are balanced by the torques generated in the joints. These torques result from manipulator bending around joints, which are considered passive elastic, such that a joint torque (τ_i) at joint (i) is given by the following relation:

$$\tau_i = K_i q_i, \tag{1}$$

where K_i is the flexural stiffness coefficient and q_i is the joint angle at joint (i) [18]. Next, the static equilibrium of the system is given by:

$$\boldsymbol{\tau}_{ext} = \mathbf{J}_{cp}^T \mathbf{w}_{ext}, \tag{2}$$

where $\mathbf{J}_{cp}^T \in \mathbb{R}^{6\times n}$ is the contact point Jacobian and $\mathbf{w}_{ext} \in \mathbb{R}^6$ denotes an external wrench on the manipulator body. This wrench can be decomposed into a force ($\mathbf{F}_{ext} \in \mathbb{R}^3$) and a moment ($\mathbf{M} \in \mathbb{R}^3$). In this study, the external moment at the i^{th} contact point is assumed to be null, i.e, we assume that the contact occurs at a point. Furthermore, the bending moment induced by the external force at joints preceding the contact point in the kinematic chain is obtained from the FBG data, and since $\mathbf{M}$ = 0,

$$\boldsymbol{\tau}_{ext} = \mathbf{J}_{cp}^T \begin{bmatrix} \mathbf{F}_{ext} \\ \mathbf{0}_3 \end{bmatrix}. \tag{3}$$

This formulation will be used in combination with shape information (q_i) derived from FBG sensor measurements. Knowing the manipulator curvature and its bending direction through the FBG sensor data, the manipulator shape is reconstructed using a numerical method which approximates the manipulator with a number of points (l_i) as described by [18]. In the following subsection, we illustrate how to calculate the external forces $\mathbf{F}_{ext}$, and how to consider these forces on multiple contact points on the manipulator body, given by the 3D coordinates of the FBG sensor positions.

D. Joint torque identification

Deriving the reconstructed positions of the FBG sensors and the surrounding manipulator body, it is possible to determine the position and coordinates of the joints of the manipulator within an environment with pre-defined curvature and known geometry. Any contact point is assumed to be known for external loads so that the Jacobian for the contact point ($\mathbf{J}_{cp}$) can be determined through the forward kinematics of the PRB model. Furthermore, if an external force $\mathbf{F}_{ext}$ acts at the manipulator tip (a single contact point), the joint torque vector from the load is calculated using (3).

To remove and reduce near singularities in the Jacobian matrix, the external force will be estimated using the Damped Least Squares of the Jacobian,

$$\begin{bmatrix} \hat{\mathbf{F}}_{ext} \\ \mathbf{0}_3 \end{bmatrix} = (\mathbf{J}_{cp}^T)_{DLS} \boldsymbol{\tau}_{ext}, \tag{4}$$

where $(.)_{DLS}$ denotes the numerically computed Damped Least Squares matrix using the Singular Value Decomposition (SVD) of $\mathbf{J}_{cp}$ [27], and $\boldsymbol{\tau}_{ext}$ is calculated from (1). Thus, the external force $\hat{\mathbf{F}}_{ext}$ is estimated using the PRB model. Consequently, in the case of n contacts between the manipulator and the environment, the contribution to a joint torque vector from the load on the i^{th} joint is given by:

$$\boldsymbol{\tau}_{ext} = \sum_{i=1}^{n} \mathbf{J}_{i_{cp}}^T \begin{bmatrix} \mathbf{F}_{i_{ext}} \\ \mathbf{0}_3 \end{bmatrix}. \tag{5}$$

Once the joint torque vector is known, the forces acting on each joint can be calculated using (4).

E. Joint stiffness identification

The manipulator is assumed to be an externally loaded incompressible beam that experiences pure bending. In order to describe the manipulator elasticity, each joint is assigned a flexural stiffness coefficient that is associated with the corresponding joint angle (q_i). The stiffness coefficient is defined for each degree of freedom. The general model derived above needs to be fitted to the system being analyzed here, hence the K_i values in (1) need to be determined.

This stiffness is determined experimentally due to the unavailability of accurate data on the manipulator material properties. The experimental setup consists of the same manipulator used in the final experiments, positioned on a plane, with a fixed base. The manipulator tip is connected to a rigid string with its end attached to a 3-axis force sensor (K3D40, Mesysteme AG, Henningsdorf, Germany), which is connected to the robotic end-effector. The end-effector is positioned in seven different known poses, which in turn deflects the manipulator body to a certain angle. The flexural stiffness coefficients are calculated as:

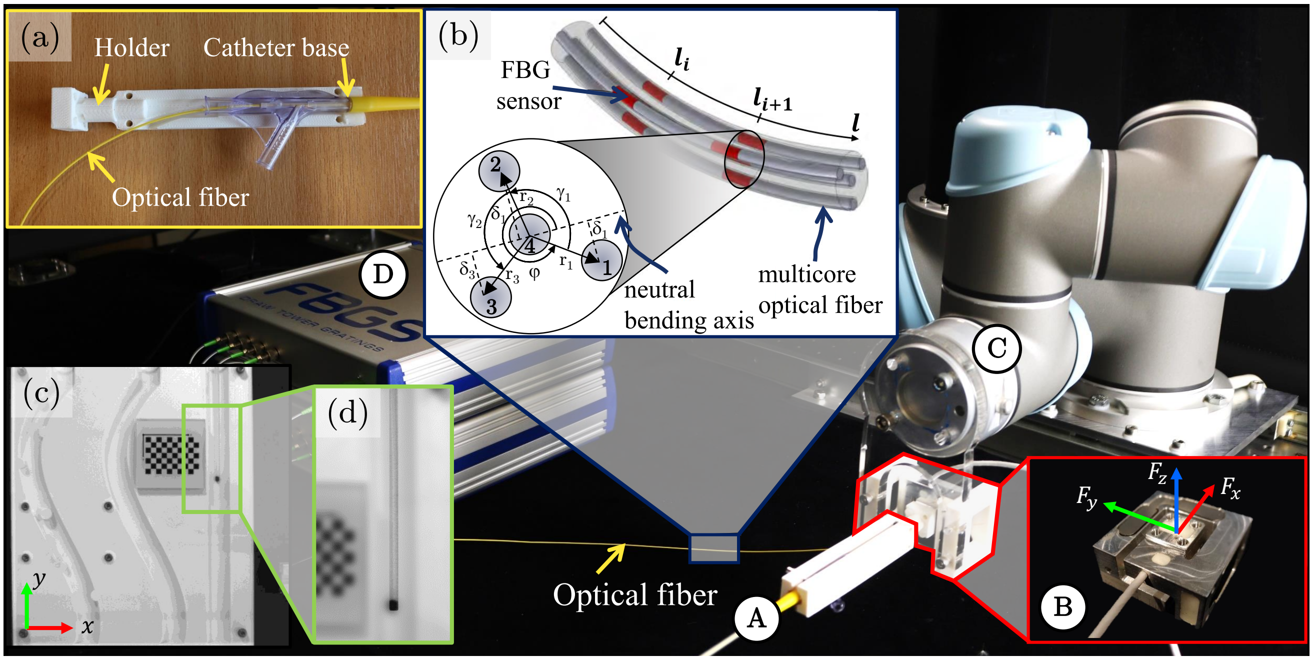

Fig. 3: Experimental setup: An endovascular catheter, (A), is connected to a K3D40 force sensor (Mesysteme AG, Henningsdorf, Germany), (B). The force sensor is used to validate the reconstructed forces experienced on the catheter body (F_x, F_y and F_z). It is connected to a serial manipulator end-effector (C). Data from Fiber Bragg Grating (FBG) sensors are retrieved using an FBG-Scan 804D interrogator (FBGS Technologies GmbH, Jena, Germany), (D). *Insets: (a)* The catheter base is fixed within a 3D-printed holder. *(b)* The fiber (with length l) used for shape sensing has four cores and each core has 32 FBG sensors (i). The cross-section is composed of 4 fibers (1), (2), (3) and (4). The distances from the center of the manipulator to the center of these fibers are r_1, r_2 and r_3, respectively. Next, γ_1 is the angle from r_1 to r_2, and γ_2 is the angle from r_2 to r_3. The perpendicular distances between the neutral bending axis and center of fibers are δ_1, δ_2, and δ_3, respectively. *(c)* The 3D printed mock-up represents a vessel environment comprising three different paths: a curved path with obstacles, a curved path, and a straight path. *(d)* The catheter segment and tip (painted black) are displayed in the straight path.

$$\mathbf{K} = \begin{bmatrix} q_1^1 & & \\ & \ddots & \\ & & q_n^1 \\ q_1^j & & \\ & \ddots & \\ & & q_n^j \\ q_1^m & & \\ & \ddots & \\ & & q_n^m \end{bmatrix}^{\dagger} \begin{bmatrix} {\tau_1}^1 \\ \vdots \\ {\tau_n}^1 \\ \vdots \\ {\tau_1}^j \\ \vdots \\ {\tau_n}^j \\ \vdots \\ {\tau_1}^m \\ \vdots \\ {\tau_n}^m \end{bmatrix} = \begin{bmatrix} K_1 \\ \vdots \\ K_i \\ \vdots \\ K_{31} \end{bmatrix}, \qquad (6)$$

where $(.)^{\dagger}$ denotes the Moore-Penrose pseudoniverse of the diagonal block matrix, whose diagonal elements denote joint angles (i = 1,...,n) associated to each trial (j =1,...,m), where m=7 and τ_i^j is the torque of joint (i) in trial (j). Using (6), the stiffness of the joints are calculated as 1.5 N·m/rad. This experiment was analyzed in the plane, hence we are tacitly assuming that the stiffness is the same in all bending directions. In order to validate the reprojection error of the PRB model, the catheter is observed by stereo view optical cameras (SONY XCD-SX90, Sony Corporation, Tokyo, Japan). After extracting video frames of the top and front view of the catheter, we use a simple correlation tracking algorithm capable of tracking the catheter tip in each frame [28]. The world-position of the catheter tip is compared to its reconstructed FBG coordinates, which delivers a mean reprojection error of 0.28 pixels (position error of 1.25 mm).

III. EXPERIMENTS

This section describes the experimental setup, the performed experiments and the procedure to reconstruct the external forces acting on the catheter body and tip.

A. Experimental setup

The experimental setup (Fig. 3) consists of a single-lumen endovascular catheter made from Polyethylene terephthalate (PET) which is connected to a serial manipulator end-effector (Model UR5, Universal Robots, Odense, Denmark). The serial manipulator system employs a native URScript interface of the UR5 to communicate with the embedded position controller. This controller executes the motion of the UR5 upon receiving a pose command, expressed as a position and angle-axis orientation, hence providing full control over the insertion procedure.

In order to reconstruct the shape of the catheter, it is fitted with a multicore fiber containing 32 equispaced FBG sensors. The catheter base is, furthermore, connected to the force sensor.

B. Force reconstruction experiments

A linear insertion ensures accurate positioning of the catheter base and, consequently, allows for further processing for the catheter position during the experiments. The

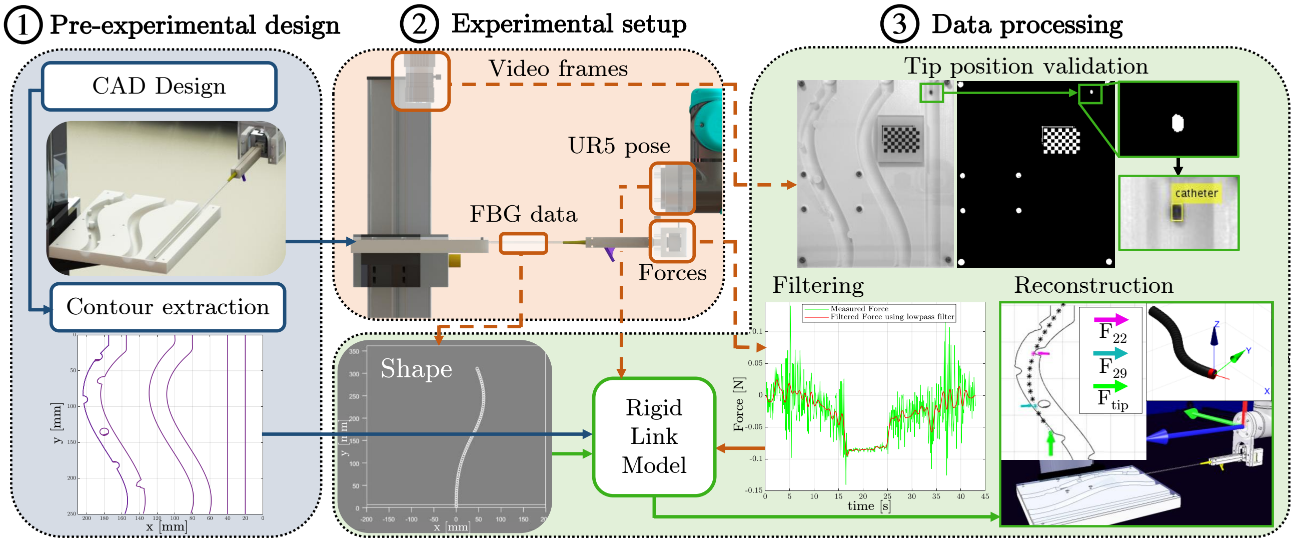

Fig. 4: Experimental workflow: (1), A catheter is inserted into a mock-up with pre-defined curvature. The entire workspace is designed using computer-aided design (CAD) technique and the mock-up is fabricated on a high-resolution 3D printer. (2), Data collected from the Fiber Bragg Grating (FBG) sensors, robotic arm (Model UR5, Universal Robots, Odense, Denmark) and K3D40 force sensor (Mesysteme AG, Henningsdorf, Germany) are used in the implemented model. (3), The procedure used to reconstruct forces on the catheter body relies on catheter shape reconstruction using multicore optical shape sensors. In order to validate the tip position, a simple tracking algorithm is implemented using adaptive thresholding (returning a binary image) in conjunction with a checkerboard calibration tool. After filtering the measured forces at the base, the reconstructed forces from the Pseudo-Rigid Body model are compared and displayed in a simulated environment.

catheter is fed into a 3D printed structure that consists of three different environments commonly found in the human arterial tree - a straight branch, a curved artery and a curved artery with blockages/abnormalities. During the experiments, the catheter is advanced into each of the paths (Fig. 3d) respectively and withdrawn again. Since the vessel is two-dimensional, forces in the z-axis are negligible, however, the reconstruction using 4 does account for that.

The strain data of the FBG sensors are collected during the entire manipulator movement using a TCP/IP connection to a separate computer. Simultaneously, the catheter insertion is being recorded from stereo cameras, while the UR5 pose, forces measurements at the base of the catheter, and FBG measurements inside the catheter are being recorded at a sample rate of 100 Hz.

IV. RESULTS

In this section, we present the data processing techniques performed to implement and evaluate the reconstruction of 3D forces on the catheter body. We first describe the data collected from the components of the experimental setup. Subsequently, the results are presented. These workflow phases are represented in Fig. 4

A. Data processing

Data processing and analysis is implemented in C++14 on a computer running Linux Ubuntu 14.04.01. This processing forms part of the final phase of the experimental workflow. 3D coordinates of 32 points which discretize the catheter from its base to the tip are extracted from the FBG sensors. Next, measurements obtained from the force sensor (consisting of 3D forces recorded at the catheter base) are filtered and used to represent the ground truth of contact forces acting on the catheter tip and along its body.

Joint positions are collected from the UR5, which are used to derive Cartesian coordinates that act as the reference position for the catheter base frame. In order to validate the proposed PRB model of the continuum manipulator, the catheter is modeled using the arm-type and robotics toolbox (MATLAB R2017b, The MathWorks, Inc., Massachusetts, United States). The entire setup is designed on computer-aided design software (Solidworks 2017, Dassault Systemes, Tennessee). This design contains, amongst others, the exact dimensions of the experimental setup apparatus in order to implement distributed control architecture in V-REP. Moreover, this simulator contains a full robot kinematic model of the UR5 and experimental setup. Catheter joint coordinates obtained from FBG strain measurements and features from the 3D setup are processed simultaneously in order to identify the contact points between the catheter body and the vessel mock-up. Consequently, this allows us to pinpoint the points at which the reconstructed forces are indicated. In the following sub-section, the force sensor measurements are compared to the forces estimated from the PRB model described in Section II.

B. Results

The magnitude of the external forces measured from the force sensor and the model are compared for the three trajectories: straight, curved and curved with obstacles. Fig. 5 shows the results of the comparison between actual forces, versus the reconstructed forces. These results indicate that the model can accurately reconstruct interaction forces along 3 axes, with a recorded mean reconstruction error of 0.02 N and a root-mean-square error (RMSE) of 0.03 N. It is

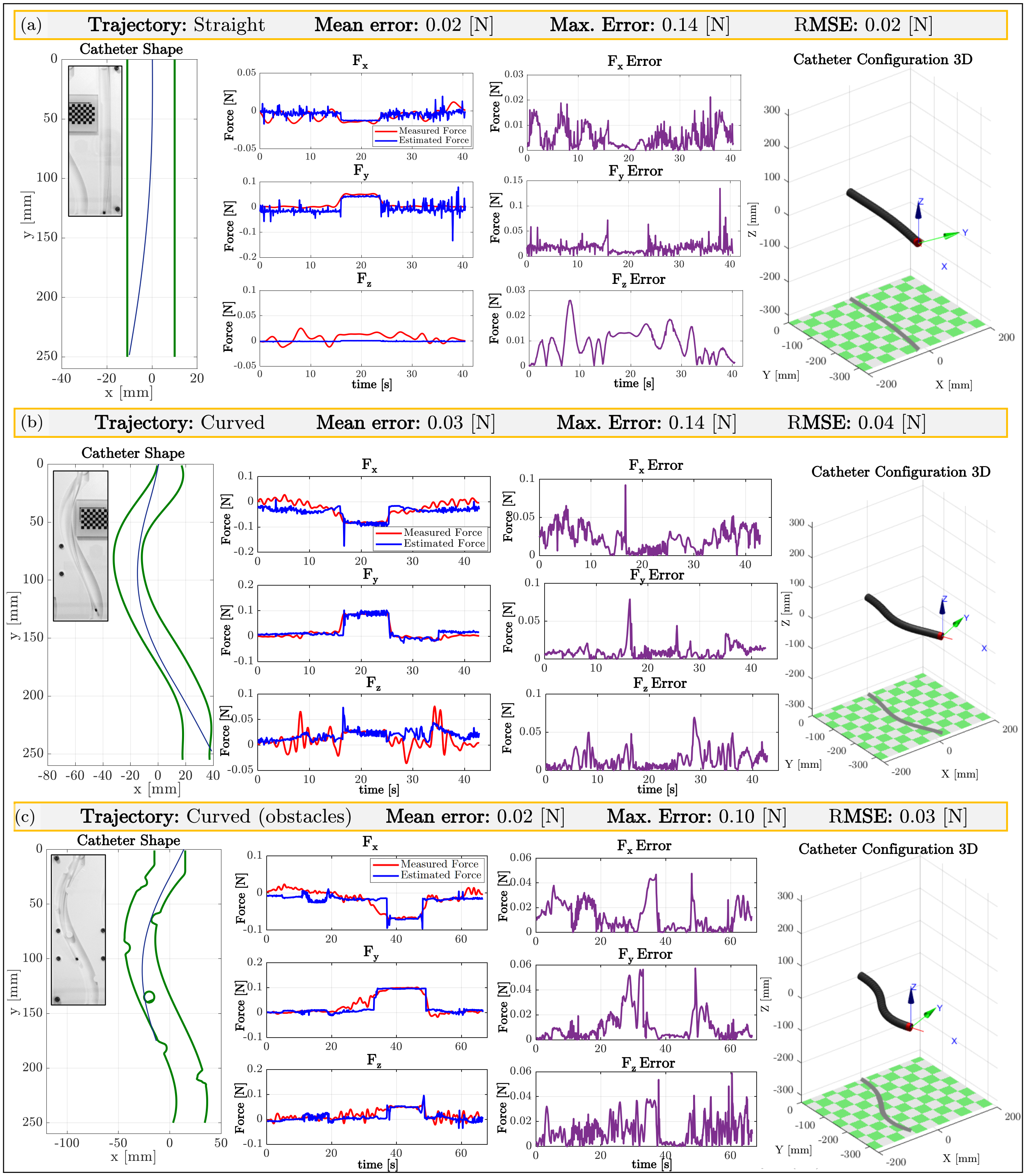

Fig. 5: The endovascular catheter is inserted into a mock-up vessel environment along three different trajectories - (a) straight, (b) curved, and (c) curved with obstacles. For each experiment, the reconstructed catheter shape is shown after full insertion. Next, the measured forces in three dimensional (3D) space are compared with the reconstructed interaction forces acting along the catheter body. The mean, maximum and root-mean-square errors (RMSE) are summarized above each set of figures. The reconstructed 3D catheter model is indicated on the right. *Real-time results can be viewed in the accompanying video.*

observed that this error is mainly present when the catheter is not in contact with its environment, and in this absence of contact, noisy force measurements occur. The norm of the error is highly reduced when contact occurs. These results are incorporated into a visualization tool developed in V-REP and showing the entire setup including the movement of UR5 with the attached force sensor and catheter. Moreover, Fig. 4 illustrates how the contact forces are indicated on the catheter.

V. CONCLUSIONS & FUTURE WORK

This study presents a novel approach to estimate the interaction forces on a catheter tip and along its body with its surrounding mock-up environment, by analyzing the changes in the shape of the catheter. A PRB model describes the manipulator shape by a serial chain of rigid-links connected by flexible rotational joints. As opposed to studies implementing single-core fibers to measure catheter tip forces, this model uses strains obtained from multicore FBG fibers spanning the entire catheter body and force measurements at the catheter base. This involved no design implementation on the catheter itself, thereby allowing us to reconstruct forces on a simple 6 Fr catheter. Although in this preliminary work the point of contact is assumed to be known, the proposed method is structurally made to include contact point identification. This is the subject of current research. Experimental validation demonstrates an RMSE value of 0.03 N and a mean reconstruction error of 0.02 N.

Besides the identification of contact points using only shape information, future studies shall include the design of an interface which concurrently shows the catheter shape inside a phantom model using a novel image fusion system. The reconstructed forces can be visualized to the clinician in real-time in an applicable user interface. For surgical interventions, this approach can be used to warn the clinician when a catheter reaches dangerously high interaction forces within the body. Furthermore, the steering experiments in this study took place inside a nondeformable mock-up in a static condition, and thus it is not clinically-relevant. To comply with clinical relevance, the study will be repeated under ultrasound guidance with a soft-tissue environment.

REFERENCES

[1] C. M. Heunis, J. Sikorski, and S. Misra, "Flexible instruments for endovascular interventions," *IEEE Robotics & Automation Magazine*, vol. 25, no. 3, pp. 71–82, 2018.

[2] K. Takashima, R. Shimomura, T. Kitou, H. Terada, K. Yoshinaka, and K. Ikeuchi, "Contact and friction between catheter and blood vessel," *Tribology International*, vol. 40, no. 2, pp. 319–328, 2007.

[3] P. Polygerinos, D. Zbyszewski, T. Schaeffter, R. Razavi, L. D. Seneviratne, and K. Althoefer, "MRI-compatible fiber-optic force sensors for catheterization procedures," *IEEE Sensors Journal*, vol. 10, no. 10, pp. 1598–1608, 2010.

[4] C. R. Wagner, N. Stylopoulos, and R. D. Howe, "The role of force feedback in surgery: analysis of blunt dissection," *Proceedings of the 10th Symposium on Haptic Interfaces for Virtual Environment and Teleoperator Systems*, pp. 68–74, Orlando, USA, March 2002.

[5] D. Shin, T. Kim, and H.-U. Kim, "Development of tri-axial fiber bragg grating force sensor in catheter application," *IEEE International Symposium on Medical Measurements and Applications (MeMeA)*, pp. 1–5, Rome, Italy, June 2018.

[6] E. Aranda-Michel, J. Yi, J. Wirekoh, N. Kumar, C. N. Riviere, D. S. Schwartzman, and Y.-L. Park, "Miniaturized robotic end-effector with piezoelectric actuation and fiber optic sensing for minimally invasive cardiac procedures," *IEEE Sensors Journal*, vol. 18, no. 12, pp. 4961–4968, 2018.

[7] B. Zhao and C. A. Nelson, "Sensorless force sensing for minimally invasive surgery," *Journal of medical devices*, vol. 9, no. 4, pp. 1–14, 2015.

[8] M. Razban, J. Dargahi, and B. Boulet, "A sensor-less catheter contact force estimation approach in endovascular intervention procedures," *IEEE/RSJ International Conference on Intelligent Robots and Systems (IROS)*, pp. 2100–2106, Madrid, Spain, October 2018.

[9] M. Khoshnam, A. C. Skanes, and R. V. Patel, "Modeling and estimation of tip contact force for steerable ablation catheters," *IEEE Transactions on Biomedical Engineering*, vol. 62, no. 5, pp. 1404–1415, 2015.

[10] J. Back, T. Manwell, R. Karim, K. Rhode, K. Althoefer, and H. Liu, "Catheter contact force estimation from shape detection using a real-time cosserat rod model," *IEEE/RSJ International Conference on Intelligent Robots and Systems (IROS)*, pp. 2037–2042, Hamburg, Germany, September 2015.

[11] C. Shi, X. Luo, P. Qi, T. Li, S. Song, Z. Najdovski, T. Fukuda, and H. Ren, "Shape sensing techniques for continuum robots in minimally invasive surgery: A survey," *IEEE Transactions on Biomedical Engineering*, vol. 64, no. 8, pp. 1665–1678, 2017.

[12] C. King, M. O. Culjat, M. L. Franco, J. W. Bisley, G. P. Carman, E. P. Dutson, and W. S. Grundfest, "A multielement tactile feedback system for robot-assisted minimally invasive surgery," *IEEE Transactions on Haptics*, vol. 2, no. 1, pp. 52–56, 2009.

[13] U. Kim, D.-H. Lee, W. J. Yoon, B. Hannaford, and H. R. Choi, "Force sensor integrated surgical forceps for minimally invasive robotic surgery," *IEEE Transactions on Robotics*, vol. 31, no. 5, pp. 1214–1224, 2015.

[14] U. Seibold, B. Kubler, and G. Hirzinger, "Prototype of instrument for minimally invasive surgery with 6-axis force sensing capability," *IEEE International Conference on Robotics and Automation (ICRA)*, pp. 496–501, Barcelona, Spain, April 2005.

[15] A. Trejos, R. Patel, and M. Naish, "Force sensing and its application in minimally invasive surgery and therapy: a survey," *Proceedings of the Institution of Mechanical Engineers, Part C: Journal of Mechanical Engineering Science*, vol. 224, no. 7, pp. 1435–1454, 2010.

[16] S. Sefati, F. Alambeigi, I. Iordachita, R. H. Taylor, and M. Armand, "On the effect of vibration on shape sensing of continuum manipulators using fiber bragg gratings," *International Symposium on Medical Robotics (ISMR)*, pp. 1–6, Atlanta, USA, March 2018.

[17] K. Yokoyama, H. Nakagawa, D. C. Shah, H. Lambert, G. Leo, N. Aeby, A. Ikeda, J. V. Pitha, T. Sharma, R. Lazzara, and W. Jackman, "Novel contact force sensor incorporated in irrigated radiofrequency ablation catheter predicts lesion size and incidence of steam pop and thrombus," *Circulation: Arrhythmia and Electrophysiology*, vol. 1, no. 5, pp. 354–362, 2008.

[18] F. Khan, R. J. Roesthuis, and S. Misra, "Force sensing in continuum manipulators using fiber bragg grating sensors," *IEEE/RSJ International Conference on Intelligent Robots and Systems (IROS)*, pp. 2531–2536, Vancouver, Canada, September 2017.

[19] T. Mattioli and M. Vendittelli, "Interaction force reconstruction for humanoid robots," *IEEE Robotics and Automation Letters*, vol. 2, no. 1, pp. 282–289, 2017.

[20] S. Haddadin, A. De Luca, and A. Albu-Schffer, "Robot collisions: A survey on detection, isolation, and identification," *IEEE Transactions on Robotics*, vol. 33, no. 6, pp. 1292–1312, 2017.

[21] E. Rohmer, S. P. Singh, and M. Freese, "V-REP: A versatile and scalable robot simulation framework," *IEEE/RSJ International Conference on Intelligent Robots and Systems (IROS)*, pp. 1321–1326, Tokyo, Japan, November 2013.

[22] R. J. Webster III, J. M. Romano, and N. J. Cowan, "Mechanics of precurved-tube continuum robots," *IEEE Transactions on Robotics*, vol. 25, no. 1, pp. 67–78, 2009.

[23] M. Mahvash and P. E. Dupont, "Stiffness control of surgical continuum manipulators," *IEEE Transactions on Robotics*, vol. 27, no. 2, pp. 334–345, 2011.

[24] T. Greigarn and M. C. Çavuşoğlu, "Pseudo-rigid-body model and kinematic analysis of MRI-actuated catheters," *IEEE International Conference on Robotics and Automation (ICRA)*, pp. 2236–2243, Seattle, USA, May 2015.

[25] J. Burgner-Kahrs, D. C. Rucker, and H. Choset, "Continuum robots for medical applications: A survey," *IEEE Transactions on Robotics*, vol. 31, no. 6, pp. 1261–1280, 2015.

[26] D. C. Rucker, B. A. Jones, and R. J. Webster III, "A geometrically exact model for externally loaded concentric-tube continuum robots," *IEEE Transactions on Robotics*, vol. 26, no. 5, p. 769, 2010.

[27] B. Siciliano, L. Sciavicco, L. Villani, and G. Oriolo, "Robotics: modelling, planning and control," *Springer Science & Business Media*, 2010.

[28] Z. Pan and X. Wang, "Correlation tracking algorithm based on adaptive template update," *3rd International Congress on Image and Signal Processing*, pp. 98–101, Yantai, China.